INTERNATIONAL JOURNAL FOR NUMERICAL METHODS IN FLUIDS, VOL. 12, 559–576 (1991)

FINITE ELEMENT MODELLING OF QUASI-THREE-DIMENSIONAL NEARLY HORIZONTAL FLOW

TORBJØRN UTNES

Norwegian Hydrotechnical Laboratory, N-7034 Trondheim, Norway

SUMMARY

A quasi-three-dimensional numerical model is presented and applied to some test problems with constant density. The numerical technique is based on a finite element formulation and the three-dimensional problem is factorized into one- and two-dimensional subproblems. The non-linear advection is treated by use of a weak formulation of the characteristics method and the equations are transformed to 'sigma' co-ordinates.

KEY WORDS Finite elements Quasi-three-dimensional Numerical oceanography

INTRODUCTION

There is an increased interest in the numerical modelling of three-dimensional fluid flow problems. One reason for this is of course the improved computer capabilities available. On the other hand, it is usually desirable to simplify the formulations whenever physically reasonable in order to increase the computational efficiency.

Numerical oceanography is a typical example to illustrate this point. Such problems can generally be described as nearly horizontal fluid flow problems and it is therefore reasonable to introduce the so-called hydrostatic pressure assumption. The resulting three-dimensional system can then be solved relatively efficiently compared to the complete three-dimensional formulation. The same kind of simplifications are usually relevant for computation of currents in fjords, lakes and rivers.

The literature on such quasi-three-dimensional numerical models has increased over the last few years. Many of these models are related to mesoscale oceanographic problems where stratification is an important parameter.[1–6] Some models have also been applied to the solution of homogeneous quasi-three-dimensional flows.[7,8] However, whether the density is assumed constant or not, the remaining problem of solving the equations of motion is the same.

The dominant part of the literature is related to finite difference models, but some exceptions can be found where finite element[7–9] and spectral models[10] have been used. For applications in areas with highly irregular geometry, such as fjords and coastal areas, great grid flexibility is advantageously. For this reason a finite element formulation has been chosen. The model equations are the quasi-three-dimensional equations referenced above and the applications shown are for homogeneous flow, although the formulation includes stratification for later use.

0271–2091/91/060559–18$09.00

Received July 1989
Revised May 1990

MODEL EQUATIONS

Quasi-three-dimensional equations

The basic mathematical formulation is given by the three-dimensional Navier–Stokes equations with the continuity equation included. The class of problems considered here is characterized by a turbulent flow with horizontal dominant mean velocity, and the vertical component of the momentum equation can therefore be reduced to a hydrostatic pressure equation to first order. By introducing the Reynolds-averaging procedure, these equations are transformed to expressions for mean values of the variables over the turbulent fluctuations. The Reynolds stresses are further simplified by introducing scalar diffusion coefficients, and the following equations are finally obtained:

horizontal momentum equations

$$\partial u/\partial t+\partial(uu)/\partial x+\partial(vu)/\partial y+\partial(wu)/\partial z=fv-\partial\Phi/\partial x+A_h\nabla^2u+\partial(A_v\partial u/\partial z)/\partial z, \tag{1}$$

$$\partial v/\partial t+\partial(uv)/\partial x+\partial(vv)/\partial y+\partial(wv)/\partial z=-fu-\partial\Phi/\partial y+A_h\nabla^2v+\partial(A_v\partial v/\partial z)/\partial z, \tag{2}$$

where

$$\Phi=p_{atm}/\rho_0+g\zeta-g\int_z^\zeta[(\rho_0-\rho)/\rho_0]\mathrm{d}z; \tag{3}$$

continuity equation

$$\partial u/\partial x+\partial v/\partial y+\partial w/\partial z=0. \tag{4}$$

The notation is as follows: (u, v, w) denote the velocity components in the Cartesian co-ordinate directions (x, y, z) respectively, where z is positive upwards; ρ is the fluid density and ρ_0 a reference density; p is the pressure and p_{atm} atmospheric pressure; ζ is the water elevation; h is the depth measured from the mean surface; A_h and A_v are the horizontal and vertical diffusivities respectively for turbulent mixing of the momentum; f is the (constant) Coriolis parameter; ∇^2 is the two-dimensional Laplacian operator in the (x, y) plane.

We transform these equations to 'sigma' co-ordinates in order to include the surface and bottom geometry easily and to allow for the same number of vertical levels all over the computational domain. The transformation from (x, y, z) to (ξ, η, σ) co-ordinates is defined by

$$\sigma=(\zeta-z)/H, \qquad \xi=x, \qquad \eta=y, \qquad \tau=t, \qquad \text{where} \quad H=h+\zeta. \tag{5}$$

In these new co-ordinates the following equations of motion can be derived:

$$\partial(Hu)/\partial\tau+\partial(Huu)/\partial\xi+\partial(Hvu)/\partial\eta+H\partial(\omega u)/\partial\sigma=Hfv-H\partial\Phi/\partial\xi+H(\partial\zeta/\partial\xi+\sigma\partial H/\partial\xi)\partial\Phi/\partial z+HA_h\nabla^2u+H^{-1}\partial(A_v\partial u/\partial\sigma)/\partial\sigma, \tag{6}$$

$$\partial(Hv)/\partial\tau+\partial(Huv)/\partial\xi+\partial(Hvv)/\partial\eta+H\partial(\omega v)/\partial\sigma=-Hfu-H\partial\Phi/\partial\eta+H(\partial\zeta/\partial\eta+\sigma\partial H/\partial\eta)\partial\Phi/\partial z+HA_h\nabla^2v+H^{-1}\partial(A_v\partial v/\partial\sigma)/\partial\sigma. \tag{7}$$

Note that the Laplacian operator for the horizontal diffusion has not been transformed. The transformation of this operator will formally contain some cross-derivatives in addition to the two-dimensional Laplacian in the (ξ, η) plane. However, for the class of problems considered the horizontal diffusion will be of minor importance and the higher-order terms can therefore be neglected.

In (6) and (7) a new vertical velocity component, $\omega = D\sigma/Dt$, has been introduced. The transformed continuity equation takes the form

$$\partial\zeta/\partial\tau + \partial(Hu)/\partial\xi + \partial(Hv)/\partial\eta + \partial(H\omega)/\partial\sigma = 0. \tag{8}$$

By integration of this equation, the following expression is obtained for ω:

$$H\omega = \int_{\sigma}^{0} [\partial(Hu)/\partial\xi + \partial(Hv)/\partial\eta]\,d\sigma + \sigma \int_{-1}^{0} [\partial(Hu)/\partial\xi + \partial(Hv)/\partial\eta]\,d\sigma. \tag{9}$$

Vertically averaged equations

By taking the vertical mean of equations (6)–(8) we obtain the following two-dimensional vertically averaged equations:

$$\partial(Hu_a)/\partial\tau + \partial(Hu_a u_a)/\partial\xi + \partial(Hv_a u_a)/\partial\eta = Hfv_a - gH\partial(\zeta+q)/\partial\xi - (H/\rho_0)\partial p_{atm}/\partial\xi + HA_h\nabla^2 u_a + (T_{s,\xi} - T_{b,\xi})/\rho_0, \tag{10}$$

$$\partial(Hv_a)/\partial\tau + \partial(Hu_a v_a)/\partial\xi + \partial(Hv_a v_a)/\partial\eta = -Hfu_a - gH\partial(\zeta+q)/\partial\eta - (H/\rho_0)\partial p_{atm}/\partial\eta + HA_h\nabla^2 v_a + (T_{s,\eta} - T_{b,\eta})/\rho_0, \tag{11}$$

$$\partial\zeta/\partial\tau + \partial(Hu_a)/\partial\xi + \partial(Hv_a)/\partial\eta = 0. \tag{12}$$

Here subscript 'a' refers to the vertically averaged velocity

$$(u_a, v_a) = \int_{-1}^{0} (u, v)\,d\sigma, \tag{13}$$

the baroclinic pressure contribution is

$$q = -\int_{-1}^{0} \left(\int_{\sigma}^{0} [H(\rho - \rho_0)/\rho_0]\,d\sigma \right) d\sigma \tag{14}$$

and T_s and T_b are the surface and bottom stresses respectively.

BOUNDARY CONDITIONS

The governing equations have the following boundary conditions in Cartesian and sigma coordinates:

at the free surface

$$\begin{aligned} &\rho_0 A_v(\partial\mathbf{u}/\partial z) = \rho_0 A_v H(\partial\mathbf{u}/\partial\sigma) = \mathbf{T}_s, \\ &w = \partial\zeta/\partial t + u\partial\zeta/\partial x + v\partial\zeta/\partial y \quad \text{or} \quad \omega = 0, \\ &p = p_{atm}; \end{aligned} \tag{15}$$

at the bottom

$$\begin{aligned} &\rho_0 A_v(\partial\mathbf{u}/\partial z) = \rho_0 A_v H(\partial\mathbf{u}/\partial\sigma) = \mathbf{T}_b, \\ &w = -(u\partial h/\partial x + v\partial h/\partial y) \quad \text{or} \quad \omega = 0. \end{aligned} \tag{16}$$

The bottom stress is calculated from the near-bottom velocity by use of the relations

$$\mathbf{T}_b = \rho_0 C_D |\mathbf{u}_b| \mathbf{u}_b, \qquad C_D = \max\{[0{\cdot}4/\ln(z_b/z_0)]^2, 0{\cdot}0025\}. \tag{17}$$

Subscript 'b' refers to the near-bottom position and z_0 is the bottom roughness. This formulation yields a logarithmic velocity profile in the bottom boundary layer if enough resolution is provided.[2]

Additional conditions must be specified at the lateral boundaries. The following are implemented in the model.

Closed (land) boundaries: $\mathbf{u}=\mathbf{0}$, $\partial\zeta/\partial n = T_{sn}/(\rho g H)$, where n is the normal to the boundary and T_{sn} is the normal component of the surface stress. The elevation condition follows by setting the velocity equal to zero in the non-stratified vertically averaged momentum equation.
Open boundary conditions: $\partial(\ )/\partial\tau + c\partial(\ )/\partial n = 0$ for all variables $(\ )$, where c is the phase speed calculated from the interior domain. It should be noted that open boundary conditions are generally difficult to handle for these kind of equations and various suggestions exist for alternative conditions (see e.g. Reference 11).

NUMERICAL PROCEDURE

General solution procedure

The governing equations to be solved are given by (6)–(9). In order to solve these equations we make use of a mode-splitting procedure. The two-dimensional part (in the (ξ, η) plane) of the three-dimensional variables are split in the form

$$\mathbf{u} = \mathbf{u}_a + \mathbf{u}_r, \tag{18}$$

where $\mathbf{u}_a$ is the vertically averaged velocity defined by (10)–(14) and $\mathbf{u}_r$ is the residual part. The equations for $\mathbf{u}_r$ are formally obtained by substitution of $\mathbf{u}_r = \mathbf{u} - \mathbf{u}_a$ into the governing equations (6) and (7) for $\mathbf{u}$. The resulting equations for $\mathbf{u}_r$ can be written in abbreviated form as

$$\partial H\mathbf{u}_r/\partial\tau = -\partial(H\mathbf{u}u_j)/\partial\xi_j + \partial(H\mathbf{u}_a u_{a,k})/\partial\xi_k + H^{-1}\partial(A_v\partial\mathbf{u}_r/\partial\sigma)/\partial\sigma + \mathbf{S}, \tag{19}$$

where summation over repeated indices is assumed. It should be noted that summation over j has three components while that over k has only two.

The general solution procedure for each time step is now as follows. The vertically averaged equations (10)–(12) for $(\mathbf{u}_a, \zeta)$ are solved first. These values are then substituted into the three-dimensional residual equation system (19), which can be solved for $\mathbf{u}_r$ by assuming $\mathbf{u}$ and $\mathbf{S}$ to be given explicitly from the previous time level. The total velocity field $(\mathbf{u}, \omega)$ is finally computed from equations (18) and (9).

A finite element formulation is applied to solve these equations. The domain is divided into three-dimensional elements which coincide with constant σ-values in the (ξ, η) plane and with vertical sides defined in the σ-direction. The element geometry is trilinear. The projection of these elements in the (ξ, η) plane is illustrated in Figure 2 (see later). These two-dimensional elements are used to solve the vertically averaged problem. The velocity interpolation is chosen to be biquadratic in the (ξ, η) plane and linear in the σ-direction, while the elevation is bilinear.

The numerical procedure for each of the subproblems above is specified in the following.

Solution of the vertically averaged equations

The vertically averaged equations can be written in abbreviated form as

$$\partial H\mathbf{u}_a/\partial\tau + \partial(u_j H\mathbf{u}_a)/\partial\xi_j = \mathbf{S}_a - gH\nabla\zeta \quad (j=1, 2), \tag{20}$$

$$\partial\zeta/\partial\tau + \nabla\cdot H\mathbf{u}_a = 0. \tag{21}$$

By introducing a weighted residual formulation of (20) in space and time we have

$$\int_{t_n}^{t_{n+1}} \int_{\Omega} W[\partial H\mathbf{u}_a/\partial\tau + \partial(u_j H\mathbf{u}_a)/\partial\xi_j - \mathbf{S}_a + gH\nabla\zeta]\,d\Omega\,dt = 0, \tag{22}$$

where W represents weighting functions, Ω is the space domain and the time step is limited by (t_n, t_{n+1}). After integration by parts, (22) becomes

$$\left(\int W H\mathbf{u}_a\,d\Omega\right)^{n+1} = \left(\int W H\mathbf{u}_a\,d\Omega\right)^{n} + \int_{t_n}^{t_{n+1}} \left(\int W(\mathbf{S}_a - gH\nabla\zeta)\,d\Omega\right)dt + \int_{t_n}^{t_{n+1}} \left(\int H\mathbf{u}_a(\partial W/\partial\tau + u_j\partial W/\partial\xi_j)d\Omega\right)dt + \int_{t_n}^{t_{n+1}} \left(\int W H\mathbf{u}_a u_n\,d\Gamma\right)dt, \tag{23}$$

where the superscripts n and $n+1$ denote time steps and u_n is the velocity component normal to the boundary Γ.

The weighting functions are chosen such that

$$\partial W/\partial\tau + u_j\partial W/\partial\xi_j = 0 \quad \text{on} \quad (t_n, t_{n+1}). \tag{24}$$

Equation (22) then reduces to

$$\left(\int W H\mathbf{u}_a\,d\Omega\right)^{n+1} = \left(\int W H\mathbf{u}_a\,d\Omega\right)^{n} + \int_{t_n}^{t_{n+1}} \left(\int W(\mathbf{S}_a - gH\nabla\zeta)d\Omega\right)dt + \mathrm{BI}, \tag{25}$$

where BI represents the boundary integral and the source terms can be integrated in time by any suitable method. The boundary integral need be calculated only if a Neumann-type condition is imposed and can be neglected when Dirichlet conditions are specified. With this in mind, the BI term will be omitted in the following for brevity.

The special choice of the weighting functions in (24) implies that these functions are independent of time in a frame moving with the fluid particles, i.e. these functions are transported along the streamlines. This method, which has been pioneered especially by the LNH group (Laboratoire National d'Hydraulique, EDF),[12,13] can be interpreted as a weak form of the method of characteristics. It should be noted that this treatment of the advection terms is numerically stable and one does not need to introduce any artificial diffusion.

A time-split procedure is now introduced to solve (25) together with the continuity equation (21). The variable $H\mathbf{u}_a$ is split as $H\mathbf{u}_a = H\mathbf{u}_{a1} + H\mathbf{u}_{a2}$, where $H\mathbf{u}_{a1}$ is defined by

$$\left(\int W H\mathbf{u}_{a1}\,d\Omega\right)^{n+1} = \left(\int W H\mathbf{u}_a\,d\Omega\right)^{n} + \int_{t_n}^{t_{n+1}} \left(\int W\mathbf{S}_a\,d\Omega\right)dt. \tag{26}$$

It follows that $H\mathbf{u}_a^{n+1}$ is then given by

$$\left(\int W H\mathbf{u}_a\,d\Omega\right)^{n+1} = \left(\int W H\mathbf{u}_{a1}\,d\Omega\right)^{n+1} - \int\left(\int W gH\nabla\zeta\,d\Omega\right)dt. \tag{27}$$

The last equation is the weighted residual formulation of

$$H\mathbf{u}_a^{n+1} = H\mathbf{u}_{a1}^{n+1} - \Delta t[\theta gH\nabla\zeta^{n+1} + (1-\theta)gH\nabla\zeta^n] \tag{28}$$

if the time integral is approximated by a weighted integration. The parameter $\theta = \frac{1}{2}$ gives a trapezoidal integration and the general range of θ is $0 \leqslant \theta \leqslant 1$.

The corresponding two-level time discretization of the continuity equation (21) is

$$\zeta^{n+1} = \zeta^n - \Delta t[\theta\nabla\cdot H\mathbf{u}_a^{n+1} + (1-\theta)\nabla\cdot H\mathbf{u}_a^n]. \tag{29}$$

This equation can be transformed to a Helmholtz equation for $\varkappa$ by taking the divergence of (28) and introducing the resulting expression for div $H\mathbf{u}_a^{n+1}$ into (29). In weighted residual form this transformed continuity equation takes the form

$$\int Q[1-\theta^2\Delta t^2 g\nabla\cdot H\nabla]\zeta^{n+1}\,\mathrm{d}\Omega=\int Q[1+\theta(1-\theta)\Delta t^2 g\nabla\cdot H\nabla]\zeta^n\,\mathrm{d}\Omega - \int Q\Delta t[\theta\nabla\cdot H\mathbf{u}_{a1}^{n+1}+(1-\theta)\nabla\cdot H\mathbf{u}_a^n]\,\mathrm{d}\Omega, \tag{30}$$

where Q represents weighting functions.

The equations to be solved are now given by (26), (27) and (30). For given values at time level n, the new time step is computed by first solving for the auxiliary velocity in (26), the elevation is then found from (30) and the complete velocity is finally computed from (27).

These equations are discretized according to the finite element method mentioned above, namely by using bilinear elements in the (ξ, η) plane and a mixed interpolation with biquadratic velocity and bilinear elevation. The weighting functions W in the momentum equation are chosen equal to the biquadratic interpolation functions, while the weighting functions Q in the Helmholtz equation are bilinear.

Solution of the residual velocity equations

The residual part of the equation system (19) is considered next. By applying the weak form of the characteristics method to these equations we have

$$\left(\int W H\mathbf{u}_r\,\mathrm{d}\Omega\right)^{n+1}=\left(\int W H\mathbf{u}\,\mathrm{d}\Omega\right)^n-\left(\int W H\mathbf{u}_a\,\mathrm{d}\Omega\right)^n+\int_{t_n}^{t_{n+1}}\left(\int W\mathbf{S}\,\mathrm{d}\Omega\right)\mathrm{d}t + \int_{t_n}^{t_{n+1}}\left(\int[WH^{-1}\partial(A_v\partial\mathbf{u}_r/\partial\sigma)/\partial\sigma]\,\mathrm{d}\Omega\right)\mathrm{d}t. \tag{31}$$

A time-split formulation is now applied to separate source terms. The vertical diffusion is treated implicitly because of stability reasons, while the rest of the source terms are either known or explicitly treated variables. This results in the following expressions:

$$\left(\int W H\mathbf{u}_r\,\mathrm{d}\Omega\right)^*=\left(\int W H\mathbf{u}\,\mathrm{d}\Omega\right)^n-\left(\int W H\mathbf{u}_a\,\mathrm{d}\Omega\right)^n+\int_{t_n}^{t_{n+1}}\left(\int W\mathbf{S}\,\mathrm{d}\Omega\right)\mathrm{d}t, \tag{32}$$

$$\left(\int W H\mathbf{u}_r\,\mathrm{d}\Omega\right)^{n+1}=\left(\int W H\mathbf{u}_r\,\mathrm{d}\Omega\right)^*+\Delta t H^{-1}\left(\int[W\partial(A_v\partial\mathbf{u}_r/\partial\sigma)/\partial\sigma]\,\mathrm{d}\Omega\right)^{n+1}. \tag{33}$$

The weighting functions here are chosen to be biquadratic in the (ξ, η) plane and linear in the σ-direction. These equations are discretized according to the finite element formulation noted previously and can finally be written in the form

$$[\mathrm{M3}]\{\mathrm{Ur}\}^*=[\mathrm{MA3}]\{\mathrm{U}\}^n-[\mathrm{Ma3}]\{\mathrm{Ua}\}^n+[\mathrm{M3}]\{\mathrm{S}\}, \tag{34}$$

$$([\mathrm{M3}]-[\mathrm{D3}])\{\mathrm{Ur}\}^{n+1}=[\mathrm{M3}]\{\mathrm{Ur}\}^*, \tag{35}$$

where matrices are indicated by [. .] and vectors with element nodal values are denoted by {. .}.

The chosen basis functions can be factorized in tensor product form, which makes it possible to factorize the three-dimensional matrices as well. A tensor factorization of the mass matrix [M3]

and the diffusion matrix [D3] into one- and two-dimensional submatrices gives

$$[M3]=[M2]\otimes[M1], \qquad [D3]=[M2]\otimes[D1], \tag{36}$$

where index '2' refers to the two-dimensional (ξ, η) plane and '1' refers to the one-dimensional σ-direction. Similarly, the modified mass matrices (due to advection) are factorized as

$$[Ma3]=[Ma2]\otimes[M1], \quad [MA3]=[MA2]\otimes[M1]. \tag{37}$$

The latter factorization is an approximation for the matrix [MA3]. However, if the element geometry is practically unchanged by the vertical advection during one time step, this is a good approximation. Since the present equation system is derived for nearly horizontal flow, this factorization should be appropriate.

The relations (36) and (37) are substituted into equations (34) and (35), and by performing some matrix operations, the equation system can finally be reduced to the following alternating direction algorithm:

sweeps in the (ξ, η) plane over all σ-levels

$$[M2]\{Ur\}^*=[MA2]\{U\}^n-[Ma2]\{Ua\}^n+[M2]\{S\}; \tag{38}$$

sweeps in the σ-direction over all (ξ, η) points

$$([M1]+[D1])\{Ur\}^{n+1}=[M1]\{Ur\}^*. \tag{39}$$

Computational aspects

The numerical technique has been chosen in order to increase the efficiency of the code as much as possible, i.e. to minimize the computer cost without reducing the accuracy too much. Some characteristic features of the present technique are discussed below.

The two-dimensional numerical integration was performed by use of a nine-point Simpson quadrature over each element. This integration technique is relatively efficient[14] and has the attractive effect that the velocity mass matrix is diagonalized for the chosen element type. The elliptic equation for the elevation (24) was solved by a direct Gaussian elimination method together with a skyline storage technique. Since the global coefficient matrix of this equation is almost time-independent (the small time-dependent part can be expressed explicitly), this matrix needs to be factorized only once and the equation can therefore be solved efficiently during the time simulation.

The implicit part of the residual equation (34) has the form of a tridiagonal system when the vertical interpolation is linear (or pentadiagonal if the interpolation is quadratic) and can be solved efficiently by standard methods.

The application of the characteristics method in the present form requires the computation of transported elements. This has been performed by transporting the element nodes using a second-order Runge–Kutta method. The values at the transported nodes are found from a standard biquadratic interpolation over each element.

Regarding computer time, test 2 in the following section is taken as an example. The computational grid has 417 velocity nodes in the horizontal plane and seven levels in the vertical. To solve this problem, a CPU time of approximately 9 s per time step was needed on a NORD 550 computer. In linearized mode the computer time is reduced by a factor of $\frac{2}{3}$. Some preprocessing time is needed in addition to factorize the elliptic equation and compute some constant matrices before the simulation is started.

MODEL APPLICATIONS

Several computations have been performed in order to test the model. Five examples are presented in the following: three of them are compared with other known or computed results; the other two examples are presented to show certain topographic and non-linear effects which are known qualitatively.

Wind-induced velocity profile in a rectangular basin

The first example is a fully developed wind-induced circulation in a long rectangular channel which is closed at both ends. The wind stress is constant in the longitudinal direction, the bottom friction is neglected, there is no rotational effect and the vertical eddy viscosity is constant. With these conditions the analytical solution of the velocity profile is easily found to be a parabolic function of z. This simple problem was computed with $h = 1$ m, $T_s = 3\ \mathrm{N\,m^{-2}}$, $\rho = 1000\ \mathrm{kg\,m^{-3}}$ and $A_v = 10^{-3}\ \mathrm{m^2\,s^{-1}}$. The numerical result is compared with the analytical solution in Figure 1 and shows excellent agreement with only six vertical levels. The numerical error for this case is limited to approximately 1%.

Wind-driven circulation in a parabolic basin

This problem is a generalization of the previous one. A constant wind stress is applied to a nearly circular closed basin with parabolic-varying bottom topography. The horizontal geometry and the computational grid are shown in Figure 2. The maximum depth at the centre is 10 m and the boundary depths are 3 m. The specified wind stress is $0{\cdot}1\ \mathrm{N\,m^{-2}}$ in the y-direction, the vertical eddy viscosity is $0{\cdot}001\ \mathrm{m^2\,s^{-1}}$ and the quadratic bottom friction coefficient is 0·0025. The three-dimensional grid has 361 velocity nodes in the horizontal plane and eight levels and the computations were performed with a time step $\Delta t = 300$ s. The model was run in linearized form and the results are shown in Figures 3–5. Isolines for the elevation are shown in Figure 3 and the surface and (near) bottom velocities are shown in Figures 4 and 5 respectively. These results are in qualitative agreement with other computations and experiments.[7,15] In these computations no

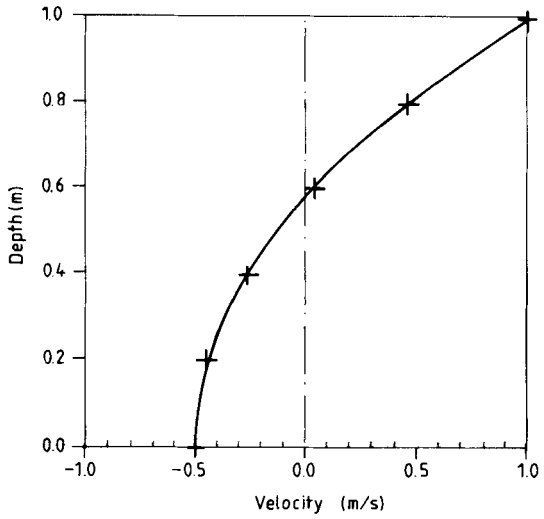

Figure 1. Wind-induced circulation in a closed channel. Comparison of analytical (——) and numerical (+) solution

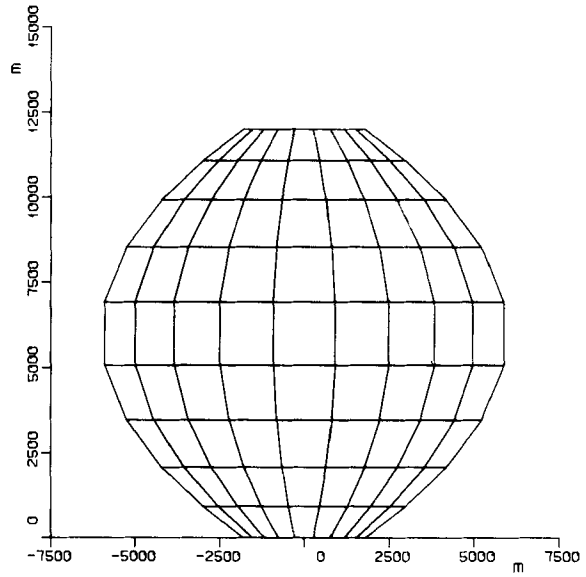

Figure 2. Geometry and computational grid for test 2

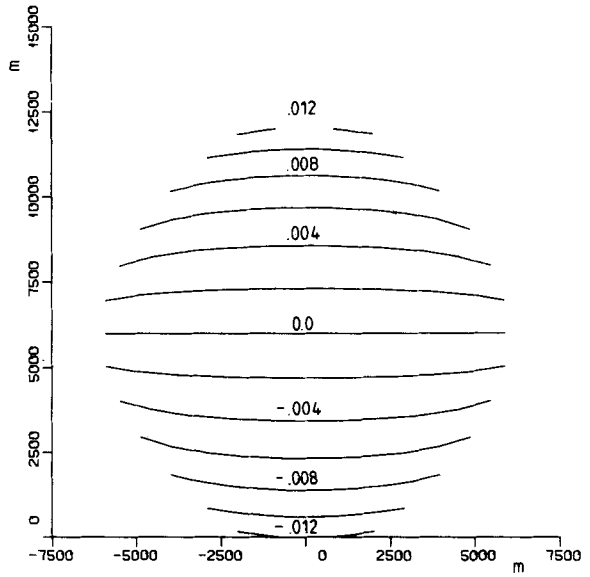

Figure 3. Surface elevation. The isoline increments are 0·002 m

Coriolis effect was included, in accordance with the references noted above, although there is a certain rotational influence present for the chosen geometrical dimensions.

One additional observation may be noted. Numerical oscillations have previously been observed in certain finite element models, especially for problems with variable bathymetry like the present one, and have led to alternative numerical formulations.[7,16] The present results show

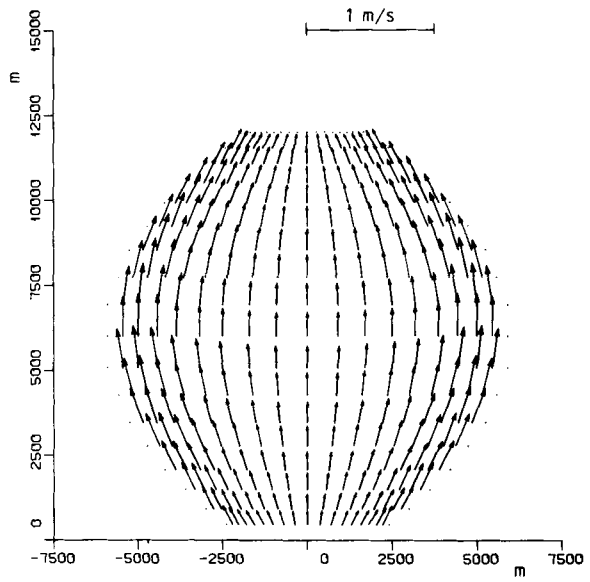

Figure 4. Surface velocity field for test 2

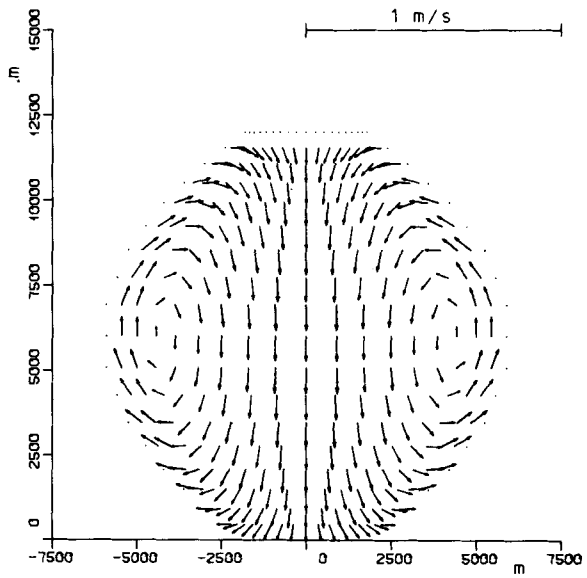

Figure 5. Near-bottom velocity field for test 2

a smooth elevation and no tendency of node-to-node oscillations. No artificial smoothing has been used and the horizontal diffusion was set to zero in these computations.

Jet-like flow through a basin

This problem was constructed in order to study the non-linear effects more closely. The general geometry is similar to the previous one, but here with a narrow inlet at one side and a similar

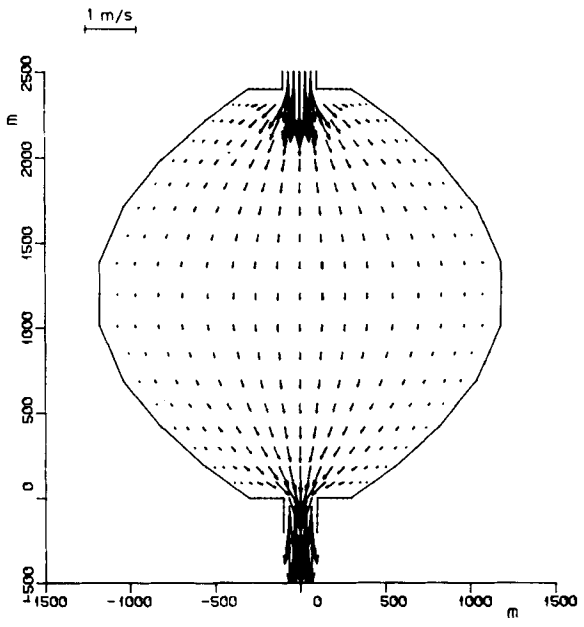

Figure 6. Geometry and linear velocity field for test 3. The velocity vectors represent vertically averaged values

outlet at the opposite side. The inlet and outlet velocities are specified as the only forcing mechanism, with a uniform value of 1 $m\,s^{-1}$. The horizontal dimensions are as shown in Figure 6 and the depth is constant and equal to 10 m. The vertical and horizontal diffusion coefficients are 0·001 and 5 $m^2\,s^{-1}$ respectively, the bottom friction is the same as in the previous test and no Coriolis effect is included. The computational grid has 417 velocity nodes in the horizontal plane and seven vertical levels and the time step was chosen as $\Delta t = 30$ s.

The model was first run in linearized form and the results from this case are shown in Figure 6. Since the vertical variations are relatively small, these results are given in vertically averaged form here. The non-linear terms were then included and the corresponding results are shown in Figure 7. It is seen that the non-linear effects have changed the flow completely. The jet-like inlet flow is now passing through the basin without being spread in the same manner as for the linear case. One can also observe that large recirculation eddies have developed which are situated approximately symmetrically on both sides of the vertical symmetry line. Results at three cross-sections are given in Figure 8.

The problem was recomputed using a two-dimensional vertically averaged version of the model and the result for this case is shown in Figures 9. By comparing Figures 7 and 9 it is seen that the three-dimensional model gives vertically averaged velocities very similar to the two-dimensional ones. Some minor differences can be observed and these may be attributed mainly to the bottom friction, which is calculated differently in the two models. A similar test has previously been reported by Benque *et al.*[17] for a two-dimensional vertically integrated model. Their result shows the same jet and recirculation trends as the present one.

Driven cavity flow

Non-linear effects have previously been studied by use of several large-scale three-dimensional or quasi-three-dimensional models. However, it seems difficult to find quantitatively well-

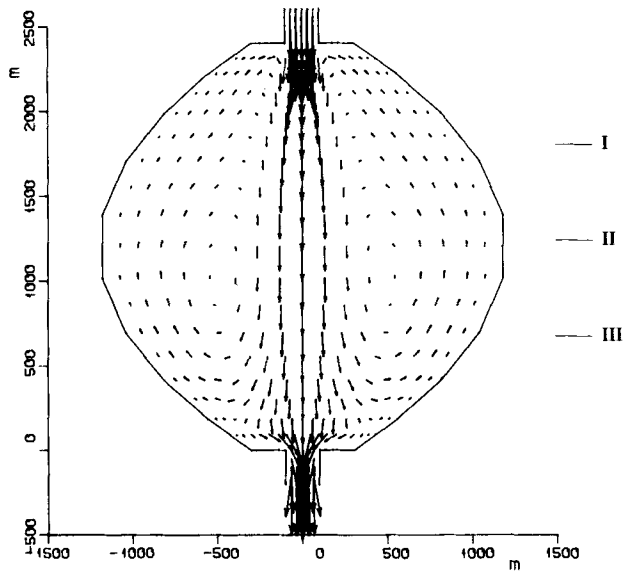

Figure 7. Non-linear velocity field computed from the three-dimensional model. The vectors represent the vertically averaged values.

established solutions of relatively simple 'benchmark' tests. Alternatively, if the two-dimensional part of the model is changed to a Navier–Stokes solver, there exist several well-documented non-linear tests. This method may reveal the accuracy of the horizontal part of the non-linear terms, which is the dominant part in this context. The test to be presented here is the classical driven cavity problem: the flow in a square cavity with three walls fixed (zero velocity) and the upper wall sliding to the left with constant velocity $U_0 = 1\ \mathrm{m\,s^{-1}}$. A Reynolds number $Re = U_0 L/A_h = 1000$ was chosen, where L is the length of the cavity. The computations were performed on an 18×18 grid (1369 velocity nodes) with refined elements near the walls and the time step $\Delta t = 0{\cdot}01$ s. The computed quasi-stationary velocity field is shown in Figure 10. This result was obtained after a simulation of about 30 s, when the solution became approximately steady state. One may observe a small secondary eddy at the lower right corner and an even smaller eddy is developing at the lower left. Such eddies are typical for this kind of flow problem and are well documented in the literature.[18,19]

The result compares well with other calculations, Figure 11, and it should be noted that the present grid is relatively coarse compared with the one used by Ghia *et al.*[18]

Uniform wind in a rectangular rotating basin

This problem has been studied by several authors and the present formulation has been chosen according to Jamart *et al.*[20] The dimensions of the basin are 600×1200 km with a uniform depth of 100 m. A uniform surface stress of $0{\cdot}1\ \mathrm{N\,m^{-2}}$ is applied in the negative y-direction, the Coriolis parameter is $1{\cdot}2 \times 10^{-4}$, the vertically uniform eddy viscosity is $0{\cdot}01\ \mathrm{m^2\,s^{-1}}$ and the horizontal diffusivity $10^3\ \mathrm{m^2\,s^{-1}}$. No-slip boundary conditions are applied both along the lateral boundaries

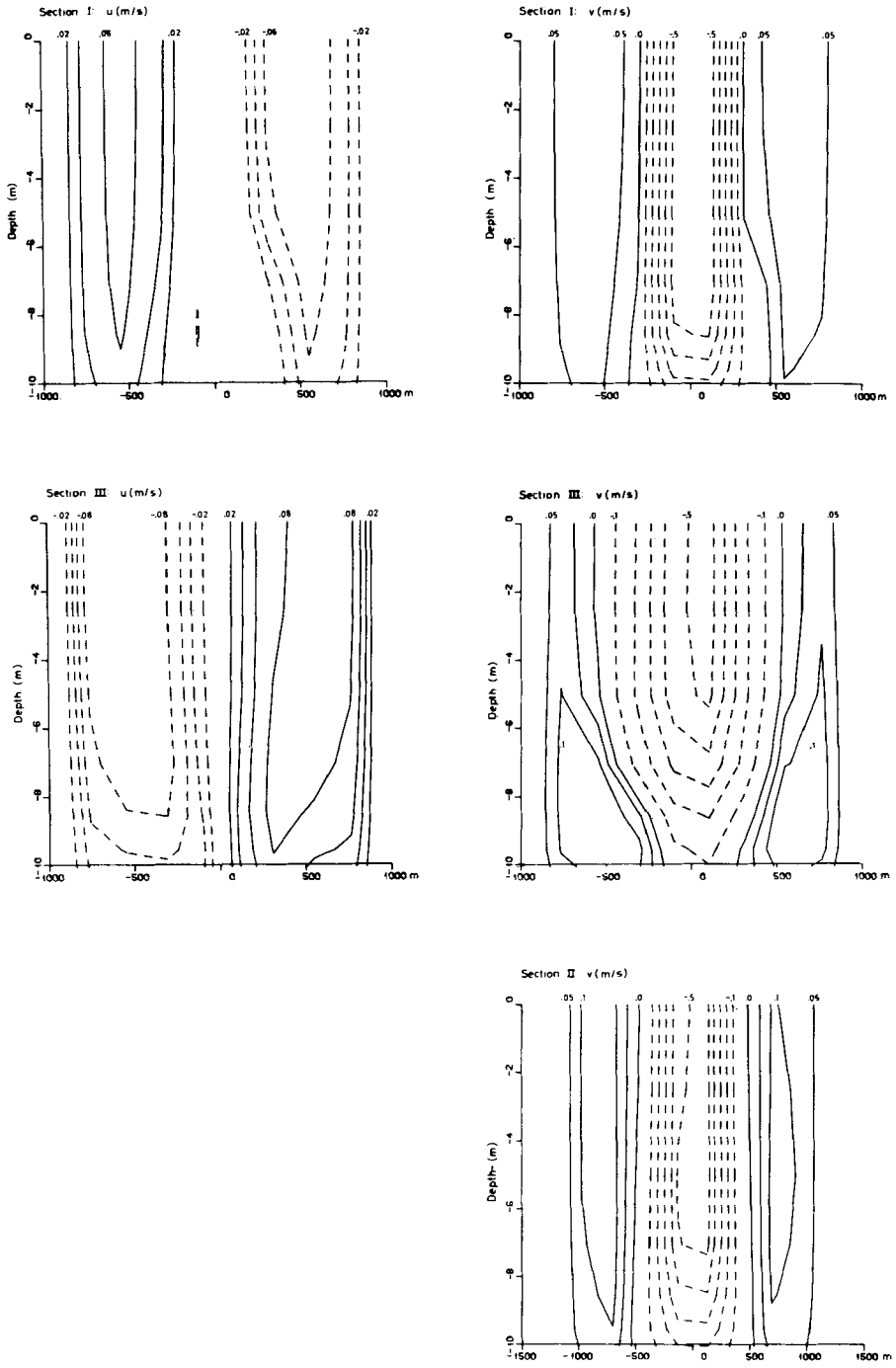

Figure 8. Velocity profiles at three cross-sections in the (x, z) plane, see Figure 7: ——, positive values; – – –, negative values. The velocity increments for u are 0·02 m s^{-1} and for v are 0·05 m s^{-1} if positive and 0·1 m s^{-1} if negative values

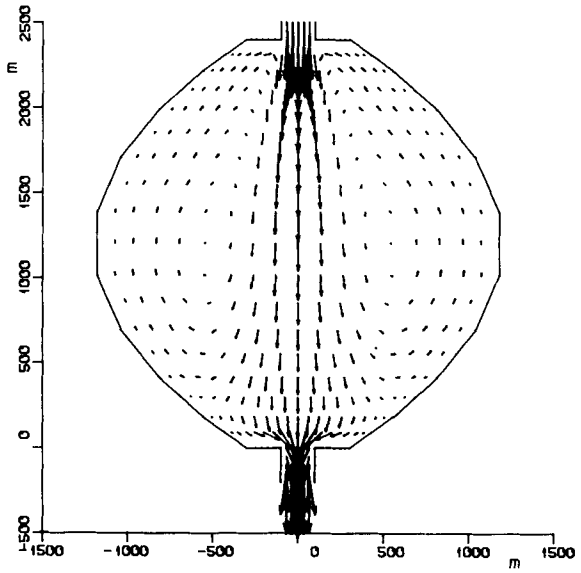

Figure 9. Non-linear velocity field computed from the two-dimensional vertically averaged model

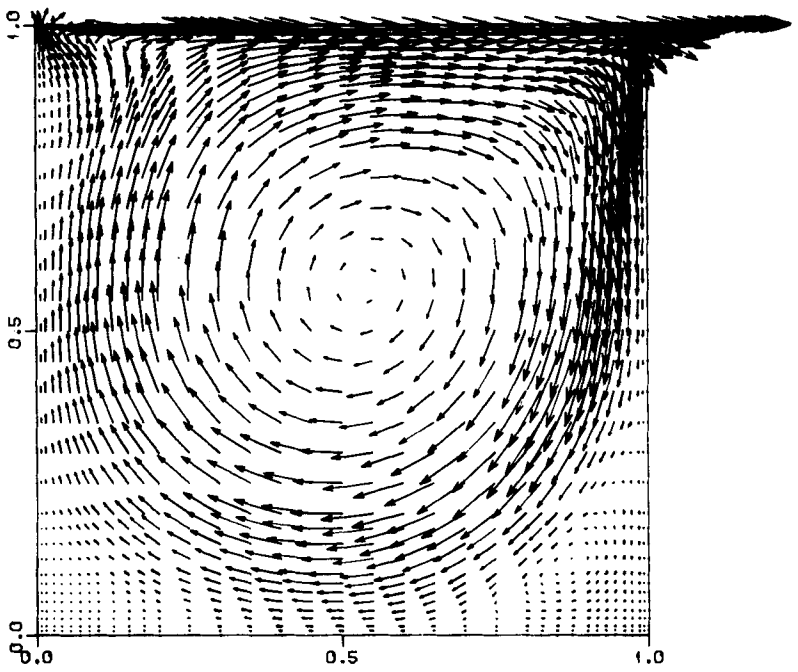

Figure 10. Computed velocity field for the cavity problem

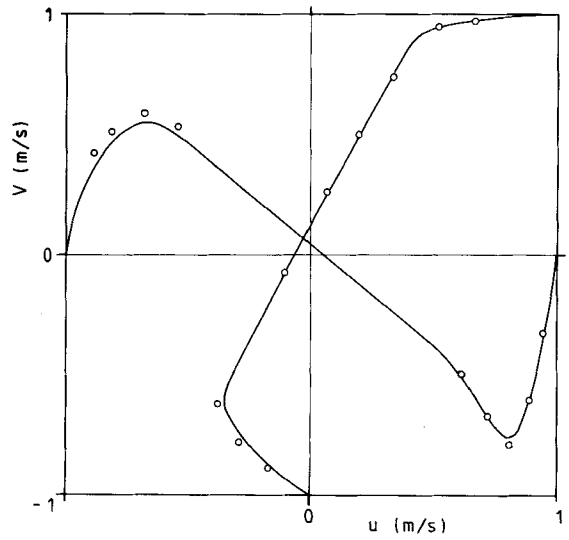

Figure 11. Comparison of velocity profiles for the cavity problem: ——, present computation; ○, Ghia *et al.*[18]

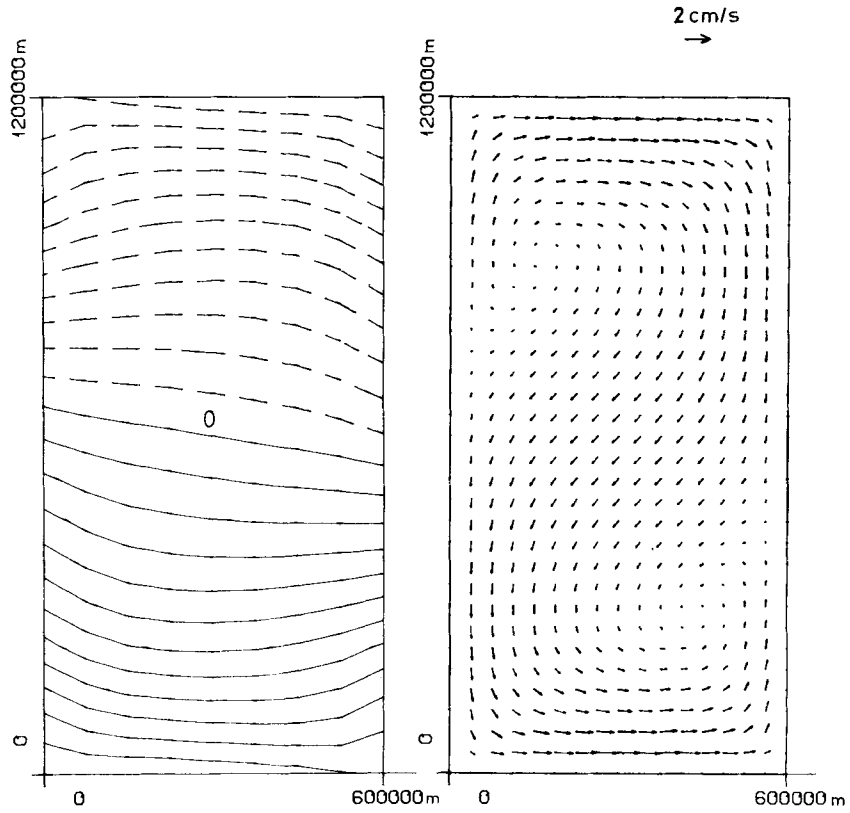

Figure 12. Results after 12 h for test 5. Left: isolines for surface elevation, 1 cm increments. Right: vertically averaged velocity

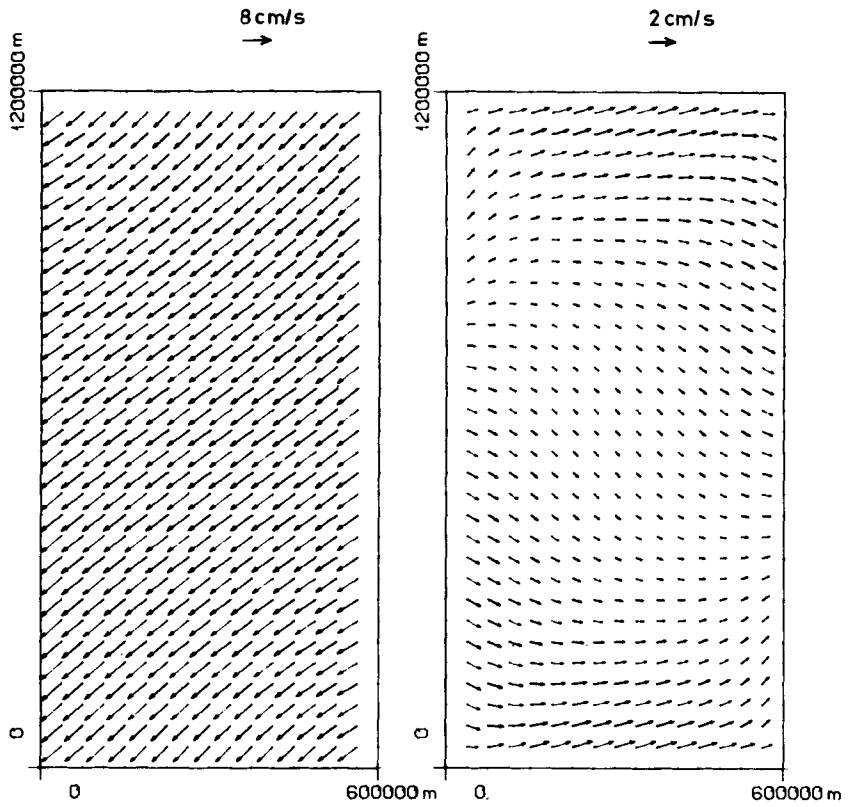

Figure 13. Results after 12 h. Left: horizontal velocity at the surface. Right: horizontal velocity 10 m above the bottom

and the bottom. The surface stress is applied impulsively and the simulation was run for about 30 h with $\Delta t = 10$ min. Examples of results at $t = 12$ h are shown in Figures 12 and 13 for elevation, mean velocity, surface and near-bottom velocities. These figures correspond to Figures 2 and 3 in Reference 20. The agreement is relatively good between those results and the present ones. A representative comparison is given in Figure 14, which shows the time evolution of the elevation at a fixed point in space. The present computation shows a somewhat higher elevation and there is a small phase difference between the two results, but the overall agreement is satisfactory.

In addition to the examples shown, it may be mentioned that the two-dimensional linear part of the model has previously been tested on several problems documented elsewhere.[21]

CONCLUDING REMARKS

The aim of this work has been to present a quasi-three-dimensional numerical model and show the results of some test problems. The experience from these tests is generally positive. The results are reasonably good and the computational algorithm is relatively efficient. Although the model is at present limited to homogeneous flow, the main difficulties with the handling of the equations of motion have been addressed.

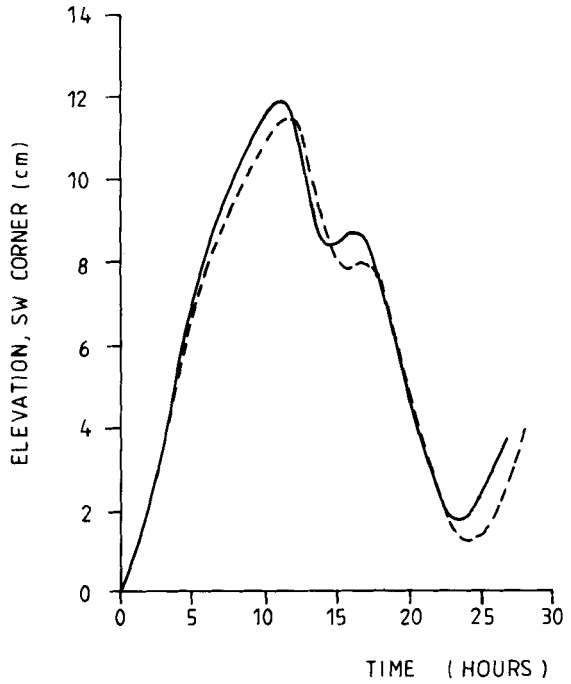

Figure 14. Comparison of elevation evolution at the southwest corner of the basin: ——, present model; – – – –, Jamart *et al.*[20]

There are several other aspects which need to be considered: the representation of the vertical turbulence, the inclusion of stratification, etc. Some of these extensions will be the topic of a future project.

ACKNOWLEDGEMENTS

This work has been supported by Konsesjonsavgiftsfondet (Fund of License Fees). I am indebted to Prof. T. McClimans for reviewing the manuscript.

REFERENCES

1. J. O. Backhaus and D. Hainbucher, 'A finite difference general circulation model for shelf seas and its application to low frequency variability on the north european shelf', in J. C. J. Nihoul and B. M. Jamart (eds), *Three-dimensional Models of Marine and Estuarine Dynamics, Elsevier Oceanography Series, Vol. 45*, 1987, pp. 221–243.
2. A. F. Blumberg and H. J. Herring, 'Circulation modelling using orthogonal curvilinear coordinates', in J. C. J. Nihoul and B. M. Jamart (eds), *Three-dimensional Models of Marine and Estuarine Dynamics, Elsevier Oceanography Series, Vol. 45*, 1987, pp. 55–88.
3. I. D. James, 'A general three-dimensional eddy-resolving model for stratified seas', in J. C. J. Nihoul and B. M. Jamart (eds), *Three-dimensional Models of Marine and Estuarine Dynamics, Elsevier Oceanography Series, Vol. 45*, 1987, pp. 591–608.
4. Y. P. Sheng and H. L. Butler, 'Modeling coastal currents and sediment transport', *Proc. 18th Coastal Engineering Conf. ASCE*, Cape Town, 1982, in B. L. Edge, (ed.), Coastal Engineering, Vol. I, 1983, pp. 1127–1148, American Society of Civil Engn., New York.
5. D. Slagstad, 'A 4-dimensional physical model of the Barents Sea', *Sintef Report STF48 F87013*, Trondheim-NTH, 1987.

6. J. C. Swanson, M. L. Spaulding, J.-P. Mathisen and Ø. O. Jensen, 'A three dimensional boundary fitted coordinate hydrodynamic model: Part 1. Development and testing', in press.
7. J. P. Laiblè, 'A finite element/finite difference wave model for depth varying nearly horizontal flow', *Adv. Water Resources*, **7**, 2–14 (1984).
8. I. P. King, 'Strategies for finite element modelling of the three dimensional hydrodynamic systems', *Adv. Water Resources*, **8**, 69–76 (1985).
9. M. Kawahara and M. Kobayashi, 'Multiple level finite element analysis and its applications to tidal current flow in Tokyo Bay', *Appl. Math. Modelling*, **7**, 197–211 (1983).
10. A. M. Davies, 'Mathematical formulation of a spectral circulation model', *Advanced Physical Oceanographic Numerical Modelling, NATO ASI Series, Series C: Mathematical and Physical Sciences, Vol. 186*, 1985, pp. 391–409.
11. L. P. Røed and C. K. Cooper, A study of various open boundary conditions for wind-forced barotropic numerical ocean models', in J. C. J. Nihoul and B. M. Jamart (eds), *Three-dimensional Models of Marine and Estuarine Dynamics, Elsevier Oceanography Series, Vol. 45*, 1987, pp. 305–335.
12. J.-P. Benque, G. Labadie and J. Ronat, 'A new finite element method for Navier–Stokes equations, coupled with a temperature equation', *Finite Element Flow Analysis*, University of Tokyo Press and North-Holland, Amsterdam, pp. 295–302, 1982.
13. J.-M. Hervouet, 'Application of the method of characteristics in their weak formulation to solving two-dimensional advection equations on mesh grids', *EDF Report R 41/85.22*, 1985.
14. A. Staniforth and C. Beaudoin, 'On the efficient evaluation of certain integrals in the Galerkin FE method', *Int. j. numer. methods fluids*, **6**, 317–324 (1986).
15. A. Giorgini and D. D. Gray, 'Wind-driven circulation in small shallow lakes: laboratory and computational experiments', *Technical Report 128*, Water Resources Research Center, Purdue University, 1980.
16. I. P. E. Kinnmark and W. G. Gray, 'An implicit wave equation model for the shallow water equations', *Adv. Water Resources*, **7**, 168–171 (1984).
17. J.-P. Benque, J. A. Cunge, J. Feuillet, A. Hauguel and F. M. Holly, 'New method for tidal current computation', *J. Waterway Port, Coastal and Ocean Div., Proc. ASCE*, **108**, (1982).
18. U. Ghia, K. N. Ghia and C. T. Shin, 'High-*Re* solutions for incompressible flow using the Navier–Stokes equations and a multi-grid method', *J. Comput. Phys.*, **48**, 387–411 (1982).
19. P. M. Gresho, S. T. Chan, R. L. Lee and C. D. Upson, 'A modified finite element method for solving the time-dependent, incompressible Navier–Stokes equations. Part 2: Applications', *Int. j. numer. methods fluids*, **4**, 619–640 (1984).
20. B. M. Jamart, J. Ozer and Y. Spitz, 'Bottom stress and free oscillations', in J. J. O'Brien (ed.), *Advanced Physical Oceanographic Numerical Modelling*, Reidel, Dordrecht, Holland, 1986, pp. 581–598.
21. T. Utnes, 'A finite element solution of the shallow-water wave equations', *Appl. Math. Modelling*, **14**, 20–29 (1990).